ADAPTIVE NEURAL NETWORK UNKNOWN TRAJECTORY TRACKING CONTROL FOR MARINE SURFACE VESSEL WITH CONSTRAINTS

Qiwei ZHANG[1], Xiyun JIANG[2*], Kexin ZHANG[3], Ziliao YUAN[4]

Most marine surface vessel (MSV) trajectory tracking problems ignore the output, state and input saturation constraints in the operation of the actual system. In addition, the desired/target trajectory for tracking is based on known conditions. To address these problems, this research introduced an adaptive tracking control scheme under the MSV system with constraints. The overall controller design is based on the backstepping control technology. Firstly, the parametric approach is adopted to estimate the desired trajectory. Secondly, an integral Barrier Lyapunov Function (iBLF) is used to directly handle system state constraints. Finally, using the mean-value theorem to deal with input saturation. In addition, the adaptive ability of fully tuned radial basis function neural network (FTRBFNN) is used to make system better compensate for uncertainties, and further improve the adaptive ability of the backstepping approach to uncertainties. With the proposed approach, the constraints will never be violated during the entire system, and the MSV system state is bounded. At the end of the research simulations proves the effectiveness of the proposed approach.

Keywords: Marine surface vessel; Unknown trajectory tracking; Backstepping; Constraints; Neural network

1. Introduction

The issue of the vessel trajectory tracking has received extensive attention from a large number of scholars in [1]. On one hand, notice that the desired trajectory or target trajectory information is accurately known in advance during the trajectory tracking of the vessel [2]. Considering the actual situation, the trajectory information of the vessel is unknown or unavailable in the process of trajectory tracking, so the corresponding control algorithm cannot be effectively implemented. On the other hand, it is a very challenging work to consider the output

[1] Prof., Engineering training centre, Chengdu Aeronautic Polytechnic, China, e-mail: 704859532@qq.com
[2*] Prof., School of aviation equipment manufacturing and industry, Chengdu Aeronautic Polytechnic, China, Corresponding author e-mail: jiangxiyun19870218@163.com
[3] Prof., Engineering training centre, Chengdu Aeronautic Polytechnic, China, e-mail: 676719025@qq.com
[4] Prof., School of aviation equipment manufacturing and industry, Chengdu Aeronautic Polytechnic, China, e-mail: yuanziliao1122@163.com

constraints, state constraints and physical constraints in the design of the MSV trajectory tracking control [3]. Therefore, it is very necessary to solve the constraint problems in MSV trajectory tracking control. However, the vast majority of references are devoted to solving the tracking problem with known trajectories, and do not consider unknown trajectories. To deal with the case of unknown trajectory, reference [4] considered the application of model predictive control-MPC to predict the future state quantities of the trajectory according to the current state quantities of the trajectory inputs thus solving the trajectory unknown problem. reference [5] applied Extended Kalman Filtering algorithm-EKF on the basis of Kalman Filtering to estimate the coordinates of the current moving position by using the state transfer equation, calculate the covariance matrix, and realize the dynamic tracking of the unknown target position through the two phases of prediction and update. In addition, reference [6] adopted deep learning-DL method and uses it to model and predict the trajectory data to solve a class of tracking problems with unknown trajectories.

For constraints existing in the actual system, some scholars have proposed using a BLF scheme [7]. Reference [8] combined BLF and neural network to solve the output feedback problem for a class of nonlinear systems. In view of the advantages of [8] , reference [9] combined BLF and neural network to solve the constrained problem in trajectory tracking of MSVs. To further improve the neural control scheme, reference[10] use BLF to ensure the full functionality of the Neural Networks-associated unit during the entire process of system operation. Reference [11] constructed an iBLF to directly deal with the output and state constraints of a class of perturbed uncertain nonlinear systems. In the same year, [20] proposed a control approach based on iBLF to handle the uncertain robot systems with joint space constraints. In addition, For input saturation, reference [12] mainly use anti-saturation compensation to design controllers for dynamic positioning system, underactuated system and Multiple Input Multiple Output (MIMO).

What's more, a problem that cannot be ignored in the control design process of the MSV's nonlinear system is the uncertainties in the system. To solve the uncertainties problems, intelligent control approaches such as neural networks/fuzzy systems are introduced into the control design to improve the robustness [9, 13].

The contributions of this research mainly includes the following aspects:

(1) The iBLF and trajectory reconstruction approach are introduced into control design of MSV trajectory tracking.

(2) The mean-value theorem is combined with hyperbolic tangent and Nussbaum to deal with asymmetric input saturation of a certain kind of MSV system. The FTRBFNN with better approximation characteristics is used to estimate the uncertainties of the MSV system.

(3) All the closed-loop MSV system signals are bounded by Lyapunov stability analysis.

2. Problem formulation

Mathematical model of marine surface vessel is established as follows:

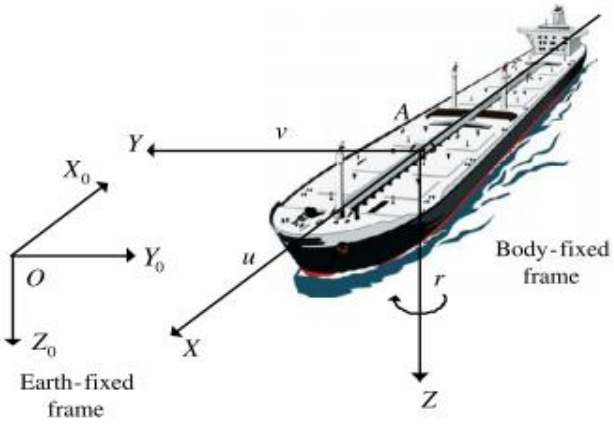

Fig. 1. The MSV in the coordinate system [12].

The three DOF MSV mathematical model is established in the O-$X_0Y_0Z_0$ and A-XYZ as follows:

$$\begin{aligned} \dot{\boldsymbol{\eta}} &= \boldsymbol{R}(\psi)\boldsymbol{\upsilon} \\ \boldsymbol{M}\dot{\boldsymbol{\upsilon}} + \boldsymbol{C}(\boldsymbol{\upsilon})\boldsymbol{\upsilon} + \boldsymbol{D}(\boldsymbol{\upsilon})\boldsymbol{\upsilon} &= \boldsymbol{\tau} + \boldsymbol{d}(\boldsymbol{\eta}, \boldsymbol{\upsilon}, t) \end{aligned} \tag{1}$$

The meaning of each parameter in Eq. (1) can be referred to reference [14]. The control objective is to design controller for Eq. (1) with saturation $\boldsymbol{\tau} \in \mathbb{R}^3$ [15], such that: 1) the vessel position $\boldsymbol{\eta}$ tracks unknown desired trajectory $\boldsymbol{\eta}_d = [x_d, y_d, \psi_d]^T$. 2) all signals are bounded and the output $\boldsymbol{\eta}$ and state $\boldsymbol{\upsilon}$ remain in the set $|\boldsymbol{\eta}| < \boldsymbol{N}_{b1}$, $|\boldsymbol{\upsilon}| < \boldsymbol{N}_{b2}$, $\forall t \geq 0$, respectively.

Assumption: For all $t \geq 0$, the estimates of $\hat{\boldsymbol{\eta}}_d$ and $\boldsymbol{\eta}_d$, as well as the estimates of $\dot{\boldsymbol{\eta}}_d$ and $\dot{\hat{\boldsymbol{\eta}}}_d$ are bounded and there exist positive constant vectors $\boldsymbol{N}_{b1}, \boldsymbol{A}_0, \boldsymbol{A}_1, \boldsymbol{A}_{01}, \boldsymbol{A}_{11}$, satisfying $|\boldsymbol{\eta}_d| \leq \boldsymbol{A}_{01} < \boldsymbol{N}_{b1}$, $|\hat{\boldsymbol{\eta}}_d| \leq \boldsymbol{A}_0 < \boldsymbol{N}_{b1}$, $|\dot{\boldsymbol{\eta}}_d| \leq \boldsymbol{A}_{11}$, $|\dot{\hat{\boldsymbol{\eta}}}_d| \leq \boldsymbol{A}_1$. Assumption limits the range of the estimated desired trajectory, which is essential for designing a feasible tracking controller.

3. Control design

The control design based on backstepping approach includes desired/target trajectory parameterization, dynamic surface, constraints and neural network approximation. The detailed design steps and analysis are as follows:

Step 1: Define the error vector as follows:

$$\boldsymbol{z}_1 = \boldsymbol{\eta} - \hat{\boldsymbol{\eta}}_d, \boldsymbol{z}_2 = \boldsymbol{\upsilon} - \boldsymbol{\alpha}_1 \tag{2}$$

where, $\boldsymbol{\alpha}_1 \in \square^3$ is the output of the first-order filter to be designed later, and $\hat{\boldsymbol{\eta}}_d(i) = \boldsymbol{f}_{di}^T(t)\hat{\boldsymbol{\omega}}_{di} + \hat{c}_{di}$ is the estimate after trajectory reconstruction, here $\hat{\boldsymbol{\eta}}_d(i)$ is the i-th element of $\hat{\boldsymbol{\eta}}_d$, $\boldsymbol{f}_{di} \in \square^l$ is a basis function vector; $\boldsymbol{\omega}_{di} \in \square^l$ and $c_{di} \in \square^l (i = 1,2,3)$ are constant parameter vector and constant parameter; $\hat{\boldsymbol{\omega}}_{di}$ and $\hat{c}_{di}$ are estimated values, respectively. For other unknown trajectory estimation method, MPC can be used to deal with the unknown trajectory problem, the essence of MPC is the use of existing models and current values, predict the future value of the system, and constantly optimize the future control volume, and ultimately make the cost function presents the smallest value of the technical means [4]. EKF can also be used, the algorithm uses the estimated signal strength value when the target is moving, combines the received signal strength value to reconstruct the mapping relationship between the distance and the signal strength, uses the state transfer equation to estimate the coordinates of the current moving position, calculates the covariance matrix, and realizes the dynamic tracking of the target position through the two phases of prediction and updating [5]. With the development of intelligent control methods, some scholars have utilized NN for data acquisition and processing, then selection and construction of the model of NN, further model training, and finally trajectory prediction to estimate the unknown trajectory.The method of DL to deal with the unknown trajectory is similar to that of NN, which belongs to the neural network prediction essentially [6, 16].

In contrast, this manuscript adopted the regular trajectory reconstruction method, and the regular trajectories include sine and cosine. It is not applicable to irregular trajectories, but the methods of MPC, EKF, NN, DL, etc. can be used for trajectory prediction. This this manuscript will subsequently deal with the prediction of irregular unknown trajectories using these methods.

In addition, we define $\tilde{\boldsymbol{\omega}}_{di} = \boldsymbol{\omega}_{di} - \hat{\boldsymbol{\omega}}_{di}$ and $\tilde{c}_{di} = c_{di} - \hat{c}_{di}$. To apply the dynamic surface control technique, the boundary layer error is introduced as follows:

$$\boldsymbol{Y} = \boldsymbol{\alpha}_1 - \boldsymbol{\alpha}_1^* \tag{3}$$

Where $\boldsymbol{\alpha}_1^* \in \square^3$ is both the virtual stabilization function to be designed and the first-order filter input.

To handle the output constraints directly, consider an iBLF candidate as

$$V_1 = \sum_{i=1}^{3} \int_0^{\boldsymbol{z}_1(i)} \frac{\boldsymbol{\beta}_1(i)\boldsymbol{N}_{b1}(i)^2 d[\boldsymbol{\beta}_1(i)]}{\boldsymbol{N}_{b1}(i)^2 - [\boldsymbol{\beta}_1(i) + \hat{\boldsymbol{\eta}}_d(i)]^2} + \frac{1}{2}\sum_{i=1}^{3} \tilde{\boldsymbol{\omega}}_{di}^T \boldsymbol{\Lambda}_i^{-1} \tilde{\boldsymbol{\omega}}_{di} + \frac{1}{2}\sum_{i=1}^{3} \tilde{c}_{di}^2 \tag{4}$$

V_1 is positive definite and continuously differentiable in the set $|\boldsymbol{\eta}| < \boldsymbol{N}_{b1}$. Where $\boldsymbol{N}_{b1}$ are the constraints; $\boldsymbol{\beta}_1(i) = \rho \boldsymbol{z}_1(i)$; $\boldsymbol{z}_1(i)$, $\boldsymbol{\beta}_1(i)$ and $\boldsymbol{N}_{b1}(i)$ $(i = 1,2,3)$ are the i-th element of vectors $\boldsymbol{z}_1$, $\boldsymbol{\beta}_1$ and $\boldsymbol{N}_{b1}$, respectively. $\boldsymbol{\Lambda}_i = \boldsymbol{\Lambda}_i^T \in \square^{3\times3}$ is positive definite design matrix;

By defining a bounded function:

$$\boldsymbol{h}_1(i) = \int_0^{\boldsymbol{z}_1(i)} \boldsymbol{\beta}_1(i)\boldsymbol{N}_{b1}^2(i) d[\boldsymbol{\beta}_1(i)] / [\boldsymbol{N}_{b1}^2(i) - [\boldsymbol{\beta}_1(i) + \hat{\boldsymbol{\eta}}_d(i)]^2],$$

and using partial integration and L'Hopital's rule to the derivative of Eq. (3), and use the Yong's Inequation for $\boldsymbol{z}_1\boldsymbol{PRY}$, we can obtain

$$\dot{V}_1 \le \boldsymbol{z}_1^T \boldsymbol{PR}\boldsymbol{z}_2 + \frac{1}{2}\boldsymbol{z}_1^T \boldsymbol{P}^T \boldsymbol{P}\boldsymbol{z}_1 + \frac{1}{2}\boldsymbol{Y}^T\boldsymbol{Y} + \boldsymbol{z}_1^T \boldsymbol{PR}\boldsymbol{\alpha}_1^* - \boldsymbol{z}_1^T \boldsymbol{\gamma}_1 \dot{\hat{\boldsymbol{\eta}}}_d - \sum_{i=1}^{3} \tilde{\boldsymbol{\omega}}_{di}^T \boldsymbol{\Lambda}_i^{-1} \dot{\hat{\boldsymbol{\omega}}}_{di} - \sum_{i=1}^{3} \tilde{c}_{di} \dot{\hat{c}}_{di} \tag{5}$$

Where, $\boldsymbol{P} = \mathrm{diag}[P_1, P_2, P_3]$, $P_i = \frac{N_{b1}^2(i)}{N_{b1}^2(i) - \eta^2(i)}$ $(i = 1,2,3)$; $\boldsymbol{\gamma}_1 = \mathrm{diag}[\gamma_1(1), \gamma_1(2), \gamma_1(3)]$.

Now, we propose virtual stabilization $\boldsymbol{\alpha}_1^*$ and adaptive law and as follows:

$$\boldsymbol{\alpha}_1^* = \boldsymbol{R}^T \left[-\boldsymbol{K}_1 \boldsymbol{z}_1 - \frac{1}{2}\boldsymbol{P}^T \boldsymbol{z}_1 + \boldsymbol{P}^{-1} \boldsymbol{\gamma}_1 \dot{\hat{\boldsymbol{\eta}}}_d \right]; \dot{\hat{\boldsymbol{\omega}}}_{di} = \boldsymbol{\Lambda}_i \left(-\delta_{1i} \hat{\boldsymbol{\omega}}_{di} + \lambda_{1i} \boldsymbol{\varphi}_{1i} \right); \dot{\hat{c}}_{di} = -\delta_{2i} \hat{c}_{di} + \lambda_{2i} \varphi_{2i} \tag{6}$$

Where, $\boldsymbol{K}_1 = \mathrm{diag}[k_{11}, k_{12}, k_{13}] > 0$, δ_{1i}, δ_{2i}, λ_{1i} and λ_{2i} are all positive design parameters; $\| \boldsymbol{\varphi}_{1i}(\boldsymbol{z}_1(i)) \| \le \phi_{1i} < \infty$, $\| \varphi_{2i}(\boldsymbol{z}_1(i)) \| \le \phi_{2i} < \infty$ are the arbitrary differentiable bounded function of $\boldsymbol{z}_1(i)$. If $\hat{\omega}_{di}$ and $\hat{c}_{di}$ are updated by Eq. (6), then $\hat{\omega}_{di}$, $\dot{\hat{\omega}}_{di}$, $\hat{c}_{di}$ and $\dot{\hat{c}}_{di}$ are bounded. Omitting of proof, readers can prove it themselves.

Through derivation, we further derive the following expression:

$$\dot{V}_1 \le -\boldsymbol{z}_1^T \boldsymbol{K}_1 \boldsymbol{P}\boldsymbol{z}_1 + \boldsymbol{z}_1^T \boldsymbol{PR}\boldsymbol{z}_2 + \frac{1}{2}\boldsymbol{Y}^T\boldsymbol{Y} - \sum_{i=1}^{3} \frac{\delta_{1i}}{4} \tilde{\boldsymbol{\omega}}_{di}^T \tilde{\boldsymbol{\omega}}_{di} - \sum_{i=1}^{3} \frac{\delta_{2i}}{4} \tilde{c}_{di}^2 + D_1 \tag{7}$$

Where, $D_1 = l_1 + l_2$, $l_1 = \Sigma_{i=1}^{3} \frac{\delta_{1i}}{2} \| \boldsymbol{\omega}_{di} \|^2 + \Sigma_{i=1}^{3} \frac{\lambda_{1i}^2 \phi_{1i}^2}{\delta_{1i}} > 0$, $l_2 = \Sigma_{i=1}^{3} \frac{\delta_{2i}}{2} c_{di}^2 + \Sigma_{i=1}^{3} \frac{\lambda_{2i}^2 \phi_{2i}^2}{\delta_{2i}} > 0$ and the coupling term $\boldsymbol{z}_1^T \boldsymbol{PR}\boldsymbol{z}_2$ will be canceled in the subsequent step.

Step 2: In this step, a first-order filter is introduced to make $\boldsymbol{\alpha}_1^*$ pass through the following first-order filter.

$$\xi \dot{\boldsymbol{\alpha}}_1 + \boldsymbol{\alpha}_1 = \boldsymbol{\alpha}_1^*, \ \boldsymbol{\alpha}_1(0) = \boldsymbol{\alpha}_1^*(0) \tag{8}$$

Where, the design constant $\xi > 0$. Since υ needs to be constrained, a Lyapunov functions candidate by augmenting V_1 with an iBLF is chosen as follows:

$$V_2 = V_1 + \sum_{i=1}^{3} \int_0^{\boldsymbol{z}_2(i)} \frac{\boldsymbol{\beta}_2(i) \boldsymbol{N}_{b2}^2(i) d[\boldsymbol{\beta}_2(i)]}{\boldsymbol{N}_{b2}^2(i) - [\boldsymbol{\beta}_2(i) + \boldsymbol{\alpha}_1(i)]^2} + \frac{1}{2}\boldsymbol{z}_2^T \boldsymbol{M}\boldsymbol{z}_2 + \frac{1}{2}\boldsymbol{Y}^T\boldsymbol{Y} \tag{9}$$

V_2 is positive definite and continuously differentiable in the set $|\upsilon| < \boldsymbol{N}_{b2}$. Where $\boldsymbol{N}_{b2}$ are the constraints; $\boldsymbol{\beta}_2(i) = \rho \boldsymbol{z}_2(i)$; $\boldsymbol{z}_2(i)$, $\boldsymbol{\beta}_2(i)$ and $\boldsymbol{N}_{b2}(i)$ are the *i*-th element of vectors $\boldsymbol{z}_2$, $\boldsymbol{\beta}_2$ and $\boldsymbol{N}_{b2}$, respectively. $|\boldsymbol{\alpha}_1(i)| < \boldsymbol{N}_{b2}(i)$ $(i = 1,2,3)$ is realized by selecting the appropriate parameter $\boldsymbol{K}_1$.

In the same way, by defining a bounded function $\boldsymbol{h}_2(i) = \int_0^{\boldsymbol{z}_2(i)} \boldsymbol{\beta}_2(i) N_{b2}^2(i) d[\boldsymbol{\beta}_2(i)] / [N_{b2}^2(i) - [\boldsymbol{\beta}_2(i) + \boldsymbol{\alpha}_1(i)]^2]$ and using partial integration and L'Hopital's rule to the derivative of Eq. (8), we have

$$\dot{V}_2 = \dot{V}_1 + \boldsymbol{z}_2^T \boldsymbol{Q}\dot{\boldsymbol{\upsilon}} - \boldsymbol{z}_2^T \boldsymbol{\gamma}_2 \dot{\boldsymbol{\alpha}}_1 + \boldsymbol{z}_2^T \left[-\boldsymbol{C}(\boldsymbol{\upsilon})\boldsymbol{\upsilon} - \boldsymbol{D}(\boldsymbol{\upsilon})\boldsymbol{\upsilon} + \boldsymbol{\tau} + \boldsymbol{d}(\boldsymbol{\eta}, \boldsymbol{\upsilon}, t) - \boldsymbol{M}\dot{\boldsymbol{\alpha}}_1 \right] + \boldsymbol{Y}^T \dot{\boldsymbol{Y}} \tag{10}$$

Where, $\boldsymbol{Q} = \mathrm{diag}[Q_1, Q_2, Q_3]$, $Q_i = \frac{N_{b2}^2(i)}{N_{b2}^2(i) - \upsilon^2(i)}$ and $\boldsymbol{\gamma}_2 = \mathrm{diag}[\gamma_2(1), \gamma_2(2), \gamma_2(3)]$.

The $\boldsymbol{\tau}$ in Eq. (10) can be expressed as $\boldsymbol{\tau} = \boldsymbol{sat}(\boldsymbol{\tau}_c) = \boldsymbol{g}(\boldsymbol{\tau}_c) + \boldsymbol{\kappa}(\boldsymbol{\tau}_c)$. We use the

piece-wise hyperbolic tangent function to describe the saturation function, then the form of $\boldsymbol{g}(\boldsymbol{\tau}_c) \in \mathbb{R}^3$ and $\boldsymbol{\kappa}(\boldsymbol{\tau}_c) \in \mathbb{R}^3$ are the same as the representation in [17]. To deal with non-affine form of $\boldsymbol{g}(\boldsymbol{\tau}_c)$, using the mean-value theorem, $\boldsymbol{g}(\boldsymbol{\tau}_c)$ satisfies $\boldsymbol{g}(\boldsymbol{\tau}_c) = \boldsymbol{g}(\boldsymbol{\tau}_c') + \boldsymbol{\Theta}(\boldsymbol{\tau}_c - \boldsymbol{\tau}_c')$. Choosing $\boldsymbol{\tau}_c' = [0,0,0]^T$, we get

$$\boldsymbol{g}(\boldsymbol{\tau}_c) = \boldsymbol{\Theta}\boldsymbol{\tau}_c \tag{11}$$

Where, $\boldsymbol{\Theta} = \mathrm{diag}[\theta_1, \theta_2, \theta_3]$, $\theta_i = \frac{\partial g_i(\boldsymbol{\tau}_C(i))}{\partial \boldsymbol{\tau}_C(i)}|_{\boldsymbol{\tau}_C(i)=\boldsymbol{\tau}_C(i)^{a_i}}$, $\boldsymbol{\tau}_c(i)^{a_i} = a_i\boldsymbol{\tau}_c(i) + (1-a_i)\boldsymbol{\tau}_c(i)'$ $(0 < a_i < 1)$.

The uncertainty in Eq. (10) is expressed in terms of $\boldsymbol{U}(\boldsymbol{Z})$, and then we approximate it with NN, and we get

$$\boldsymbol{U}(\boldsymbol{Z}) = -\boldsymbol{C}(\upsilon)\upsilon - \boldsymbol{D}(\upsilon)\upsilon + \boldsymbol{d}(\eta, \upsilon, t) - \boldsymbol{M}\dot{\alpha}_1 = \boldsymbol{W}^{*T}\boldsymbol{S}^*(\boldsymbol{Z}, \boldsymbol{\mu}^*, \boldsymbol{\sigma}^*) + \varepsilon(\boldsymbol{Z}, \boldsymbol{\mu}^*, \boldsymbol{\sigma}^*) \tag{12}$$

where $\boldsymbol{W}^* = [\boldsymbol{W}_1^*, \boldsymbol{W}_2^*, \boldsymbol{W}_3^*]$ is the ideal weight matrix; $\boldsymbol{S}^* = [\boldsymbol{S}_1^{*T}, \boldsymbol{S}_2^{*T}, \boldsymbol{S}_3^{*T}]^T$ is the ideal basis function vector; $\boldsymbol{Z} = [\upsilon^T, \boldsymbol{\alpha}_1^T, \dot{\boldsymbol{\alpha}}_1^T]^T$ is NN's input vector; $\boldsymbol{\mu}^*$, $\boldsymbol{\sigma}^*$ are the ideal center and width of basis functions $\boldsymbol{S}^*$, respectively. In addition, $\varepsilon(\boldsymbol{Z}, \boldsymbol{\mu}^*, \boldsymbol{\sigma}^*)$ satisfy $\| \varepsilon(\boldsymbol{Z}, \boldsymbol{\mu}^*, \boldsymbol{\sigma}^*) \| \le \bar{\varepsilon}$.

The time derivative of $\dot{V}_2$ is organized as

$$\begin{aligned}\dot{V}_2 \le & -\boldsymbol{z}_1^T\boldsymbol{K}_1\boldsymbol{P}\boldsymbol{z}_1 + \boldsymbol{z}_1^T\boldsymbol{P}\boldsymbol{R}\boldsymbol{z}_2 - \frac{1}{4}\sum_{i=1}^{3}\frac{\delta_{1i}}{\lambda_{\max}(\Lambda_i^{-1})}\tilde{\boldsymbol{\omega}}_{di}^T\Lambda_i^{-1}\tilde{\boldsymbol{\omega}}_{di} - \frac{1}{4}\sum_{i=1}^{3}\delta_{2i}\tilde{c}_{di}^2 + D_1 + \boldsymbol{z}_2^T\boldsymbol{Q}\dot{\upsilon} - \boldsymbol{z}_2^T\boldsymbol{\gamma}_2\dot{\alpha}_1 \\ & + \boldsymbol{z}_2^T\left[\boldsymbol{W}^{*T}\boldsymbol{S}^*(\boldsymbol{Z}, \boldsymbol{\mu}^*, \boldsymbol{\sigma}^*) + \varepsilon(\boldsymbol{Z}, \boldsymbol{\mu}^*, \boldsymbol{\sigma}^*) + \boldsymbol{\Theta}\boldsymbol{\tau}_c + \boldsymbol{\kappa}(\boldsymbol{\tau}_c)\right] + \left(\frac{1}{2} - \frac{1}{\xi} + \frac{\varpi^2}{\iota^2}\right)\boldsymbol{Y}^T\boldsymbol{Y} + \frac{\iota^2}{4}\end{aligned} \tag{13}$$

In inequation (13), $\boldsymbol{\Theta}$ is time-varying, this makes the design and analysis difficult. To solve this problem and avoid the calculation of $\boldsymbol{\Theta}^{-1}$, we introduce the Nussbaum function matrix $\boldsymbol{N} = \mathrm{diag}[N_1(\varsigma_1), N_2(\varsigma_2), N_3(\varsigma_3)]$, and the control law for $\boldsymbol{\tau}_c$ is design as

$$\begin{aligned} & N_i(\varsigma_i) = \varsigma_i^2\cos\varsigma_i, \quad \dot{\varsigma}_i = \chi_\varsigma\bar{\boldsymbol{\tau}}_c(i)\boldsymbol{z}_2(i) \\ & \boldsymbol{\tau}_c = \boldsymbol{N}\bar{\boldsymbol{\tau}}_c, \quad \bar{\boldsymbol{\tau}}_c = -\boldsymbol{Q}\dot{\upsilon} + \boldsymbol{\gamma}_2\dot{\boldsymbol{\alpha}}_1 - \boldsymbol{R}^T\boldsymbol{P}^T\boldsymbol{z}_1 - \boldsymbol{K}_2\boldsymbol{Q}\boldsymbol{z}_2 - \boldsymbol{K}_3\boldsymbol{z}_2 - \hat{\boldsymbol{W}}^T\hat{\boldsymbol{S}}(\boldsymbol{Z}, \hat{\boldsymbol{\mu}}, \hat{\boldsymbol{\sigma}}) \end{aligned} \tag{14}$$

Where, $\chi_\varsigma > 0$; $\boldsymbol{K}_2 = \mathrm{diag}[k_{21}, k_{22}, k_{23}] > 0$ and $\boldsymbol{K}_3 = \mathrm{diag}[k_{31}, k_{32}, k_{33}] > 0$ are positive definite design matrices; $\hat{\boldsymbol{W}}$, $\hat{\boldsymbol{S}}$, $\hat{\mu}$ and $\hat{\sigma}$ are the estimates of $\boldsymbol{W}^*$, $\boldsymbol{S}^*$, $\boldsymbol{\mu}^*$ and $\boldsymbol{\sigma}^*$, respectively. We define $\hat{\boldsymbol{W}} = \boldsymbol{W}^* - \tilde{\boldsymbol{W}}$, $\hat{\boldsymbol{\mu}} = \boldsymbol{\mu}^* - \tilde{\boldsymbol{\mu}}$ and $\hat{\boldsymbol{\sigma}} = \boldsymbol{\sigma}^* - \tilde{\boldsymbol{\sigma}}$. In addition, $\hat{\boldsymbol{W}} = [\hat{\boldsymbol{W}}_1, \hat{\boldsymbol{W}}_2, \hat{\boldsymbol{W}}_3]$ is the weight matrix of the NNs; $\hat{\boldsymbol{S}} = [\hat{\boldsymbol{S}}_1^T, \hat{\boldsymbol{S}}_2^T, \hat{\boldsymbol{S}}_3^T]^T$ are the estimated basis functions.

Consider the following augmented Lyapunov functions candidate

$$V_3 = V_2 + \frac{1}{2}\sum_{i=1}^{3}\tilde{\boldsymbol{W}}_i^T\boldsymbol{\Gamma}_{W_i}^{-1}\tilde{\boldsymbol{W}}_i + \frac{1}{2}\sum_{i=1}^{3}\tilde{\boldsymbol{\mu}}_i^T\Gamma_{\mu_i}^{-1}\tilde{\boldsymbol{\mu}}_i + \frac{1}{2}\sum_{i=1}^{3}\tilde{\boldsymbol{\sigma}}_i^T\Gamma_{\sigma_i}^{-1}\tilde{\boldsymbol{\sigma}}_i \tag{15}$$

Based on the properties of FTRBFNN, we have the following expression:

$$\boldsymbol{W}^{*T}\boldsymbol{S}^* - \hat{\boldsymbol{W}}^T\hat{\boldsymbol{S}} = \tilde{\boldsymbol{W}}^T\left(\hat{\boldsymbol{S}} - \boldsymbol{S}_{\hat{\mu}}'\hat{\boldsymbol{\mu}} - \boldsymbol{S}_{\hat{\sigma}}'\hat{\boldsymbol{\sigma}}\right) + \hat{\boldsymbol{W}}^T\boldsymbol{S}_{\hat{\mu}}'\tilde{\boldsymbol{\mu}} + \hat{\boldsymbol{W}}^T\boldsymbol{S}_{\hat{\sigma}}'\tilde{\boldsymbol{\sigma}} + \tilde{\boldsymbol{W}}^T\boldsymbol{S}_{\hat{\mu}}'\boldsymbol{\mu}^* + \tilde{\boldsymbol{W}}^T\boldsymbol{S}_{\hat{\sigma}}'\boldsymbol{\sigma}^* + \tilde{\boldsymbol{W}}^{*T}\boldsymbol{O}(\boldsymbol{Z}, \tilde{\boldsymbol{\mu}}, \tilde{\boldsymbol{\sigma}}) \tag{16}$$

Take the derivative of Eq. (15), and then based on Eq. (16), we design the

following adaptive law:

$$\dot{\hat{\boldsymbol{W}}}_i = \boldsymbol{\Gamma}_{\boldsymbol{W}_i}[\boldsymbol{H}_i \boldsymbol{z}_2(i) - \nu_i \,|\, \boldsymbol{z}_2(i) \,|\, \hat{\boldsymbol{W}}_i] \tag{17}$$

$$\dot{\hat{\boldsymbol{\mu}}}_i = \Gamma_{\boldsymbol{\mu}_i}[\boldsymbol{S}_{\hat{\boldsymbol{\mu}}_i}'^T \hat{\boldsymbol{W}}_i \boldsymbol{z}_2(i) - \nu_{2i} \,|\, \boldsymbol{z}_2(i) \,|\, \hat{\boldsymbol{\mu}}_i] \tag{18}$$

$$\dot{\hat{\boldsymbol{\sigma}}}_i = \Gamma_{\boldsymbol{\sigma}_i}[\boldsymbol{S}_{\hat{\boldsymbol{\sigma}}_i}'^T \hat{\boldsymbol{W}}_i \boldsymbol{z}_2(i) - \nu_{3i} \,|\, \boldsymbol{z}_2(i) \,|\, \hat{\boldsymbol{\sigma}}_i] \tag{19}$$

Where, $\nu_i > 0$, $\nu_{2i} > 0$ and $\nu_{3i} > 0$ $(i = 1,2,3)$ are design constants.

Substitute Eq. (17)-Eq. (19) into the derivative of $\dot{V}_3$ for sorting, and then apply Lemma 2 in Appendix A.1. Finally, we obtain

$$\dot{V}_3 \le -\Delta V_3 + \frac{1}{\chi_\varsigma}\sum_{i=1}^{3}\left(\theta_i N_i(\varsigma_i) - 1\right)\dot{\varsigma}_i + c \tag{20}$$

Here we can sort out Δ

$$\Delta = \min\left\{\begin{array}{l} \lambda_{\min}(\boldsymbol{K}_1), \lambda_{\min}(\boldsymbol{K}_2), \dfrac{2[\lambda_{\min}(\boldsymbol{K}_3) - 2]}{\lambda_{\max}(\boldsymbol{M})}, \xi^*, \min\left[\dfrac{\delta_{1i}}{2\lambda_{\max}(\Lambda_i^{-1})}\right] \\ \min\left(\dfrac{\delta_{2i}}{2}\right), \min\left[\dfrac{\nu_i^2 \,\|\, \boldsymbol{W}_i^* \,\|^2}{2\lambda_{\max}(\boldsymbol{\Gamma}_{\boldsymbol{W}_i}^{-1})}\right], \min\left(\dfrac{\nu_{2i}^2 \,\|\, \boldsymbol{\mu}_i^* \,\|^2}{2\Gamma_{\boldsymbol{\mu}_i}^{-1}}\right), \min\left(\dfrac{\nu_{3i}^2 \,\|\, \boldsymbol{\sigma}_i^* \,\|^2}{2\Gamma_{\boldsymbol{\sigma}_i}^{-1}}\right) \end{array}\right\} \tag{21}$$

$\xi^* = \frac{2}{\xi} - 1 - \frac{2\varpi^2}{t^2}$, $c = \Sigma_{i=1}^{3}\overline{D}_i$ $(i = 1,2,3)$. To ensure $\Delta > 0$, $\xi^* > 0$, the design matrix $\boldsymbol{K}_3$ is chosen to satisfy $\lambda_{\min}(\boldsymbol{K}_3) - 2 > 0$. Multiplying both sides of inequation (20) by $e^{\Delta t}$ and integrating inequation (20) over $[0, t]$, inequation (20) further becomes

$$V_3(t) \le \frac{c}{\Delta} + \left[V_3(0) - \frac{c}{\Delta}\right]e^{-\Delta t} + \frac{e^{-\Delta t}}{\chi_\varsigma}\int_0^t \sum_{i=1}^{3}\left(\theta_i N_i(\varsigma_i) - 1\right)\dot{\varsigma}_i e^{-\Delta\tau} d\tau \le b_0 + \frac{e^{-\Delta t}}{\chi_\varsigma}\int_0^t \sum_{i=1}^{3}\left(\theta_i N_i(\varsigma_i) - 1\right)\dot{\varsigma}_i e^{-\Delta\tau} d\tau \tag{22}$$

Where, $b_0 = V_3(0) + \frac{c}{\Delta}$.

Theorem: Consider the MSV systems (1) with the input saturation, uncertainty, and full-state constraints, under Assumptions 1. If the initial conditions satisfy $|\boldsymbol{\eta}(0)| < \boldsymbol{N}_{b1}$, $|\boldsymbol{\upsilon}(0)| < \boldsymbol{N}_{b2}$, under the virtual stabilization function $\boldsymbol{\alpha}_1^*$, the first-order filter Eq. (8), the control laws Eq. (14), and the adaptive laws Eq. (17)-Eq. (19), $\hat{\omega}_{di}$ and $\hat{c}_{di}$. If the design parameters are chosen appropriately, the system has the following properties:

1) The system full-state constraints are never violated, i.e., $|\boldsymbol{\eta}| < \boldsymbol{N}_{b1}$, $|\boldsymbol{\upsilon}| < \boldsymbol{N}_{b2}$, $\forall t \ge 0$.

2) All signals of the closed-loop system are bounded.

Proof: 1) Noting the definition of V_3 in Eq. (20), and letting b_1 be the upper bound of term $\frac{e^{-\Delta t}}{\chi_\varsigma}\int_0^t \Sigma_{i=1}^{3}\left(\theta_i N_i(\varsigma_i) - 1\right)\dot{\varsigma}_i e^{-\Delta\tau} d\tau$ and $\mathrm{F} = b_0 + b_1$, we can obtain

$$V_3(t) \le \mathrm{F} \tag{23}$$

According to the BLF, $V_3(t) \to \infty$, when $|\boldsymbol{\eta}(i)| \to \boldsymbol{N}_{b1}(i)$, $|\boldsymbol{\upsilon}(i)| \to \boldsymbol{N}_{b2}(i)$ $(i = 1,2,3)$. Due to the boundedness of $V_3(t)$, we know that $|\boldsymbol{\eta}(i)| \ne \boldsymbol{N}_{b1}(i)$, $|\boldsymbol{\upsilon}(i)| \ne \boldsymbol{N}_{b2}(i)$, i.e.,

$|\boldsymbol{\eta}(i)| < \boldsymbol{N}_{b1}(i)$, $|\boldsymbol{v}(i)| < \boldsymbol{N}_{b2}(i)$, $\forall t \geq 0$.

Proof: 2) It is easy to obtain that each term of Eq. (23) is positive, and we have inequations:

$$\frac{\boldsymbol{z}_1(i)^2}{2} \leq V_3(t) \leq \mathrm{F}, \ \frac{\boldsymbol{z}_2(i)^2}{2} \leq V_3(t) \leq \mathrm{F}, \ \frac{1}{2}\boldsymbol{z}_2^T \boldsymbol{M}\boldsymbol{z}_2 \leq V_3(t) \leq \mathrm{F} \tag{24}$$

The final convergence set of errors are as follows:

$$\| \boldsymbol{z}_1(i) \| \leq \sqrt{\frac{2c}{\Delta} + 2b_1}, \ \| \boldsymbol{z}_2(i) \| \leq \sqrt{\frac{2c}{\Delta} + 2b_1} \cap \| \boldsymbol{z}_2(i) \| \leq \sqrt{\frac{2c + 2b_1\Delta}{\lambda_{\min}(\boldsymbol{M})\Delta}}, \ i = 1,2,3 \tag{25}$$

Based on inequation (5), the virtual stabilization function $\boldsymbol{\alpha}_1^*$ is a function about $\boldsymbol{R}^T$, $\boldsymbol{z}_1$, $\boldsymbol{P}^T$, $\boldsymbol{P}^{-1}$, $\boldsymbol{\gamma}_1$, $\dot{\hat{\boldsymbol{\eta}}}_d$. Combining the form of $\boldsymbol{\alpha}_1^*$ and the first-order filter, we have $|\boldsymbol{\alpha}_1| < \boldsymbol{N}_{b2}$, while using $\dot{\boldsymbol{\alpha}}_1 = (\boldsymbol{\alpha}_1^* - \boldsymbol{\alpha}_1)/\xi$, $\xi > 0$, we can know that $\dot{\boldsymbol{\alpha}}_1$ is also bounded. From inequation (22) and Lemma 1 in Appendix A.1, it can be conveniently shown that ς_i is bounded. Because $\boldsymbol{N}$ is bounded, $\dot{\varsigma}_i$ in Eq. (14) is bounded, and we can know that $\boldsymbol{\tau}_c$ is bounded. In addition, according to inequation (22) and $\| \boldsymbol{W}_i^* \| \leq \overline{W}_i$, $\| \boldsymbol{\mu}_i^* \| \leq \overline{\mu}_i$, $\| \boldsymbol{\sigma}_i^* \| \leq \overline{\sigma}_i$, then $\tilde{\boldsymbol{W}}_i$, $\hat{\boldsymbol{W}}_i$, $\tilde{\boldsymbol{\mu}}_i$, $\hat{\boldsymbol{\mu}}_i$, $\tilde{\boldsymbol{\sigma}}_i$ and $\hat{\boldsymbol{\sigma}}_i$ are also bounded. From Eq. (17)-Eq. (19), it is readily know that $\dot{\hat{\boldsymbol{W}}}_i$, $\dot{\hat{\boldsymbol{\mu}}}_i$, $\dot{\hat{\boldsymbol{\sigma}}}_i$ are all bounded. Finally, the estimated trajectory is bounded within the desired trajectory. Consequently, all signals are bounded.

4. Simulations

In this section, to demonstrate the effectiveness of the proposed approach, the detailed model parameters are shown in [18]. We choose a general desired trajectory form similar to [19]. The output constraints and state constraints are chosen as $\boldsymbol{N}_{b1} = [5.3\mathrm{m}, 4.3\mathrm{m}, 1.05\mathrm{rad}]^{\mathrm{T}}$ and $\boldsymbol{N}_{b2} = [0.5\mathrm{m/s}, 0.5\mathrm{m/s}, 0.5\mathrm{rad/s}]^{\mathrm{T}}$, respectively. The constraint range of the control forces and moment are given as $\tau_1 \in [-20\mathrm{N}, 20\mathrm{N}]$, $\tau_2 \in [-15\mathrm{N}, 15\mathrm{N}]$, $\tau_3 \in [-5\mathrm{Nm}, 5\mathrm{Nm}]$.

The Part 1: The initial conditions and the control designed as: $\boldsymbol{\eta}(0) = [0.2\mathrm{m}, 0.2\mathrm{m}, 0\mathrm{rad}]^{\mathrm{T}}$, $\boldsymbol{v}(0) = [0\mathrm{m/s}, 0\mathrm{m/s}, 0\mathrm{rad/s}]^{\mathrm{T}}$. To approach the true disturbance, the disturbance is specified as follows, reference to [18]: The basis functions are $\boldsymbol{f}_{d1} = [\cos_1(0.1t), \cdots, \cos_l(0.1t)]^{\mathrm{T}}$, $\boldsymbol{f}_{d2} = \boldsymbol{f}_{d3} = [\sin_1(0.1t), \cdots, \sin_l(0.1t)]^{\mathrm{T}}$, The bounded function are chosen as $\boldsymbol{\varphi}_{1i}(\boldsymbol{\eta}(i)) = [\cos_1(\boldsymbol{z}_1(i)), \cdots, \cos_l(\boldsymbol{z}_1(i))]^T$ and $\varphi_{2i}(\boldsymbol{\eta}(i)) = 0.1\sin(\boldsymbol{z}_1(i))$, $(i = 1,2,3)$, where $\boldsymbol{z}_1(1) = x - x_d$, $\boldsymbol{z}_1(2) = y - y_d$ and $\boldsymbol{z}_1(3) = \psi - \psi_d$. The trajectory estimation design parameters are set as follows: $\boldsymbol{\Lambda}_i = 0.5\boldsymbol{I}_{l\times l}$, $\lambda_{11} = \lambda_{12} = \lambda_{13} = 0.1$, $\lambda_{21} = \lambda_{22} = \lambda_{23} = 0.05$, $\delta_{11} = 0.1$, $\delta_{12} = 0.5$, $\delta_{12} = 0.5$ $\hat{\boldsymbol{\omega}}_{di,j}(0) = 0$ and $\hat{c}_{di}(0) = 1$, $(i = 1,2,3; \ j = 1,2,\cdots,l)$. The controller parameters are set as follows: $\boldsymbol{K}_1 = \mathrm{diag}(0.1.0.1, 0.1)$, $\boldsymbol{K}_2 = \mathrm{diag}(1, 2, 2)$, $\boldsymbol{K}_3 = \mathrm{diag}(5, 10, 10)$. The filter time constant is set as $\xi = 0.52$, $0 < \xi^* < 0.54$. The neural network parameters are set as

$\hat{\boldsymbol{W}}_{i,j}(0)=\hat{\boldsymbol{\mu}}_{i,j}(0)=\hat{\boldsymbol{\sigma}}_{i,j}(0)=0$, $\boldsymbol{\Gamma}_{\boldsymbol{W}_i}=\boldsymbol{I}_{l\times l}$, $\boldsymbol{\Gamma}_{\boldsymbol{\mu}_i}=\boldsymbol{\Gamma}_{\boldsymbol{\sigma}_i}=0.5\boldsymbol{I}_{l\times l}$, $\nu_i=\nu_{2i}=\nu_{3i}=2.5\times10^{-5}$, $l=40$, $\chi_\varsigma=10^{-5.5}$. Compared to the standard approach, we use the same design parameters and the virtual stabilization function is designed as $\boldsymbol{\alpha}_1^*=\boldsymbol{R}^T[-(\boldsymbol{K}_1+\frac{\boldsymbol{P}^T}{2})\boldsymbol{z}_1+\dot{\hat{\boldsymbol{\eta}}}_d]$. The the control law is designed as $\boldsymbol{\tau}_c=-\hat{\boldsymbol{W}}^T\hat{\boldsymbol{S}}(\boldsymbol{Z},\hat{\boldsymbol{\mu}},\hat{\boldsymbol{\sigma}})-\boldsymbol{K}_3\boldsymbol{z}_2$. The simulation time is set to 100 seconds. Fig. 2-Fig. 12. Shows the results.

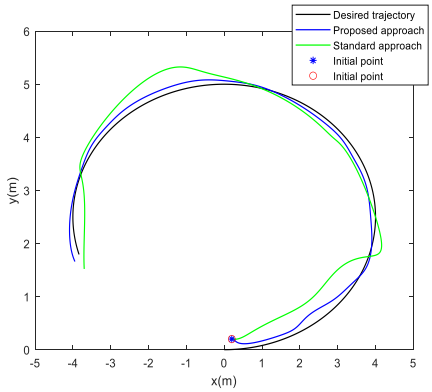

Fig. 2. Trajectory tracking curves in xy plane (Part 1).

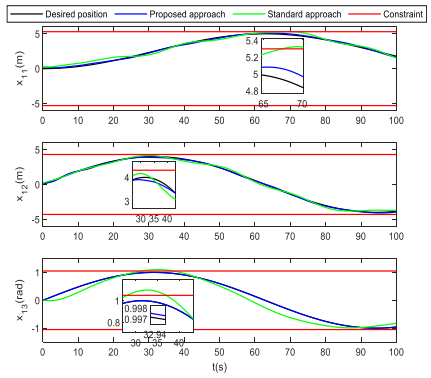

Fig. 3. The vessel position status tracking curves x_{11}, x_{12}, x_{13}.

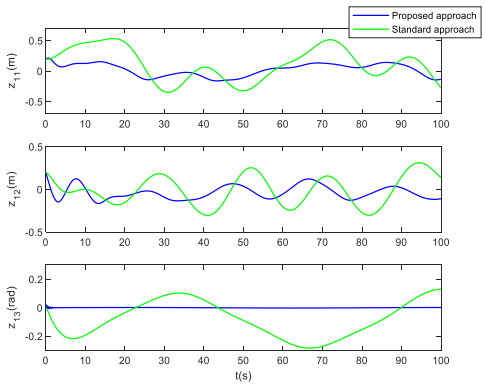

Fig. 4. The position tracking errors z_{11}, z_{12}, z_{13}.

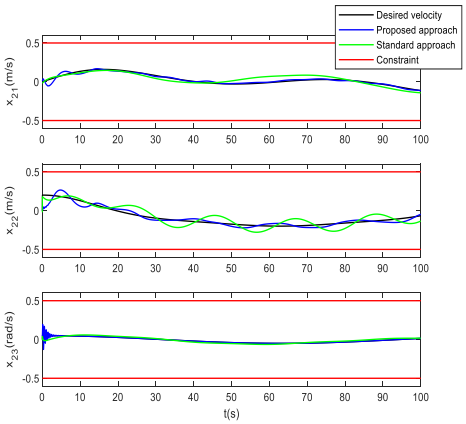

Fig. 5. The vessel velocity status tracking curves x_{21}, x_{22}, x_{23}.

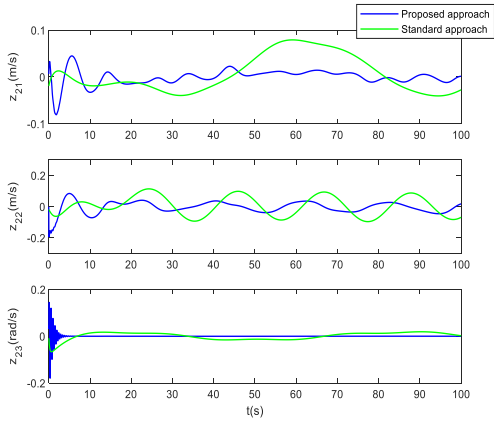

Fig. 6. The velocity tracking error z_{21}, z_{22}, z_{23}.

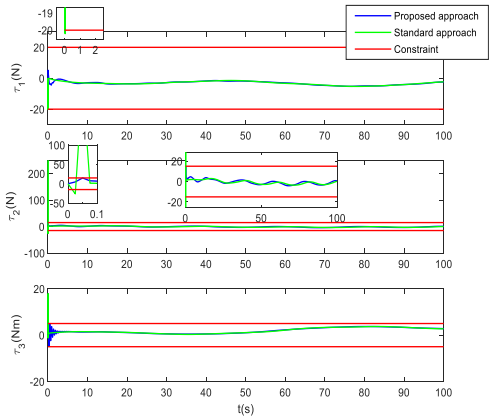

Fig. 7. Surge control force τ_1, sway control force τ_2, and yaw control moment τ_3.

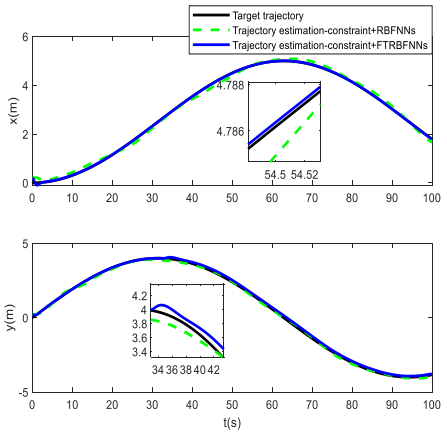

Fig. 8. Desired trajectory and desired trajectory

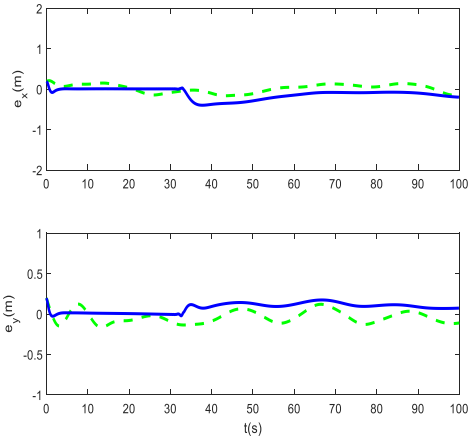

Fig. 9. Desired trajectory estimation and desired trajectory error e_x, e_y.

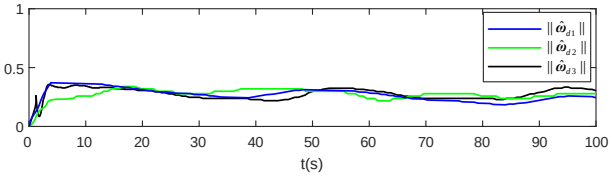

Fig. 10. The 2-norm curves of estimate trajectory parameters $\|\hat{\omega}_{d1}\|$, $\|\hat{\omega}_{d2}\|$, $\|\hat{\omega}_{d3}\|$.

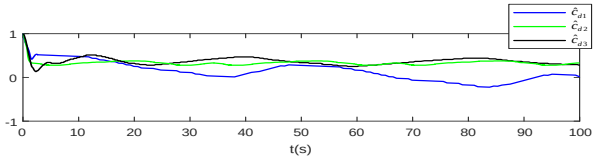

Fig. 11. The response curves of estimate trajectory parameters $\hat{c}_1$, $\hat{c}_2$, $\hat{c}_3$.

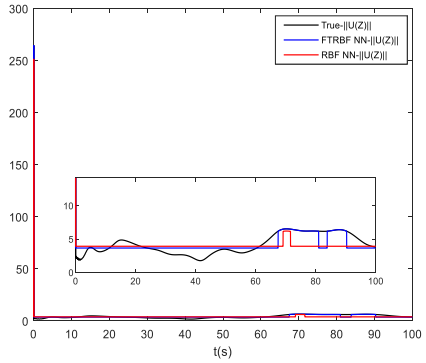

Fig. 12. System uncertainties approximation comparison.

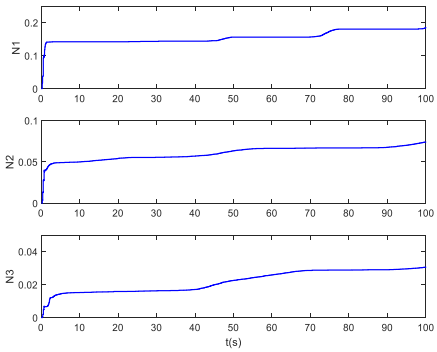

Fig. 13. Nussbaum parameters.

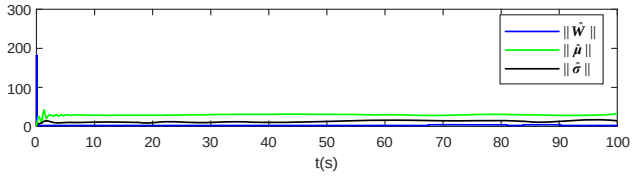

Fig. 14. The 2-norm curves of neural network estimation weight $\|\hat{W}\|$, Gaussian function center estimation value $\|\hat{\mu}\|$ and width estimation value $\|\hat{\sigma}\|$.

Fig. 2 shows that the proposed approach has a better tracking effect. In Fig. 3 at about 65-70 seconds, the proposed approach can make the surge position x_{11} within the constraints. The standard approach does not work. At about 30-40 seconds, the proposed approach can make the heading angle position x_{13} within the constraints, while the heading angle position x_{13} violates the constraints under the standard approach. Fig. 4 shows the steady-state tracking errors are closer to zero under the proposed approach. Figure 5 shows the velocity x_{21}, x_{22}, and x_{23} of Cybership II under two approaches. Fig. 6 shows the steady-state tracking errors are closer to zero under the proposed approach. Combining Fig. 3 and Fig. 4, the proposed approach ensures that both the system state variables $\boldsymbol{\eta} \Leftrightarrow \boldsymbol{x}_1$ and $\boldsymbol{\upsilon} \Leftrightarrow \boldsymbol{x}_2$ operate safely within constraints. Although the system velocity state does not violate the constraints under the standard approach, it cannot satisfy the constraint requirements in the perspective of control approach theory. Fig. 7 shows that the proposed approach effectively restrains the control force and torque, and ensures that the control force does not exceed the actual limit.

Fig. 8 and Fig. 9 show that the trajectory parameter linearization approach is used to estimate the desired trajectory very well. The estimation error fluctuates with a small amplitude around zero. Fig. 10 and Fig. 11 correspond to the change curves of the trajectory estimation parameters $\hat{\omega}_{d1}$, $\hat{\omega}_{d2}$, $\hat{\omega}_{d3}$, $\hat{c}_1$, $\hat{c}_2$ and $\hat{c}_3$, respectively. It can be seen that the change range of these parameters are bounded.

Fig. 12 shows the comparison results of the system uncertainties approximation under the two neural network approaches. It can be further seen from

Fig. 12 that FTRBFNNs has stronger online learning abilities and adaptive abilities. Fig. 13 corresponds to the changes in Nussbaum parameters. Fig. 14 corresponds to the estimated weights $\hat{w}$, base function center estimation $\hat{\mu}$ and width estimation $\hat{\sigma}$ two-norm changes. It can be seen that the range of changes are bounded.

This Part 2 is the comparison of tracking conditions under different control parameters. The trajectory estimation design parameters are set as follows: $\boldsymbol{\Lambda}_i = \boldsymbol{I}_{l\times l}$, $\lambda_{11} = \lambda_{12} = \lambda_{13} = 0.25$, $\lambda_{21} = \lambda_{22} = \lambda_{23} = 0.2$, $\delta_{11} = 0.5$, $\delta_{12} = 1$, $\delta_{12} = 1$, $\hat{\boldsymbol{\omega}}_{di,j}(0) = 0$ and $\hat{c}_{di}(0) = 1$, $(i = 1,2,3;\quad j = 1,2,\cdots,l)$, $\xi = 0.52$, $0 < \xi^* < 0.54$. $\boldsymbol{\Gamma}_{\boldsymbol{w}_i} = 1.5\boldsymbol{I}_{l\times l}$ $\boldsymbol{K}_1 = \mathrm{diag}(1,1,1)$, $\boldsymbol{K}_2 = \mathrm{diag}(15,25,25)$, $\boldsymbol{K}_3 = \mathrm{diag}(50,50,100)$, $\hat{\boldsymbol{\mu}}_{i,j}(0) = 0$, $\boldsymbol{\Gamma}_{\boldsymbol{\mu}_i} = \boldsymbol{\Gamma}_{\boldsymbol{\sigma}_i} = \boldsymbol{I}_{l\times l}$ $\hat{\boldsymbol{\sigma}}_{i,j}(0) = 0$ $\hat{\boldsymbol{W}}_{i,j}(0) = \hat{\boldsymbol{\mu}}_{i,j}(0) = \hat{\boldsymbol{\sigma}}_{i,j}(0) = 0$ $\nu_i = \nu_{2i} = \nu_{3i} = 10^{-4}$. The other parameters do not change, and the simulations time is still 100 seconds. Fig. 15-Fig. 20 shows the results.

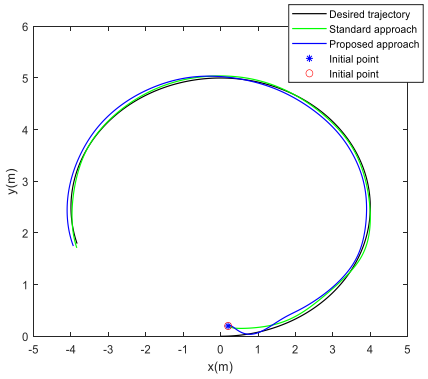

Fig. 15. Trajectory tracking curves in xy plane (Part 2).

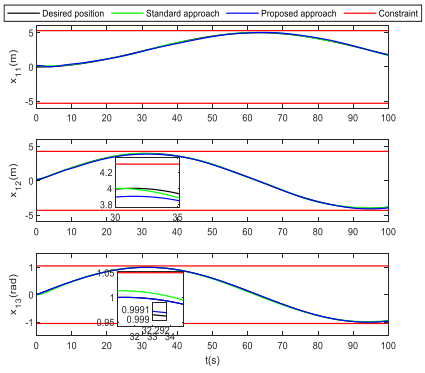

Fig. 16. The vessel position status tracking curves x_{11}, x_{12}, x_{13}.

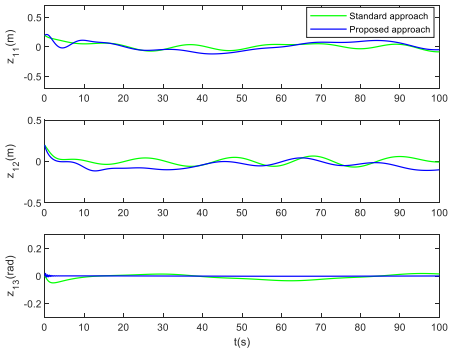

Fig. 17. The position tracking errors z_{11}, z_{12}, z_{13}.

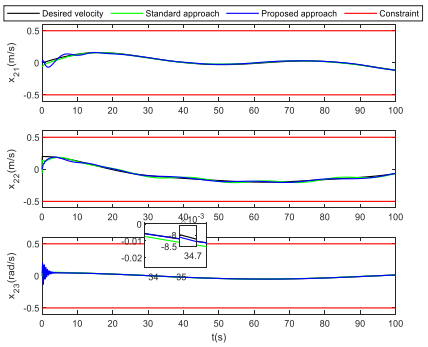

Fig. 18. The vessel velocity status tracking curves x_{21}, x_{22}, x_{23}.

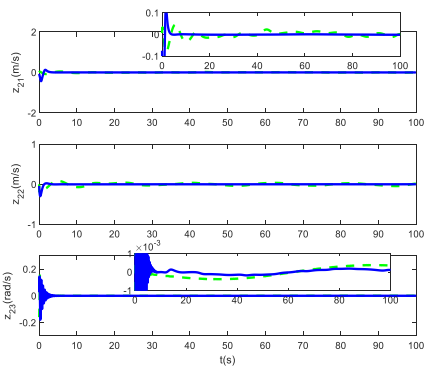

Fig. 19. The velocity tracking error z_{21}, z_{22}, z_{23}.

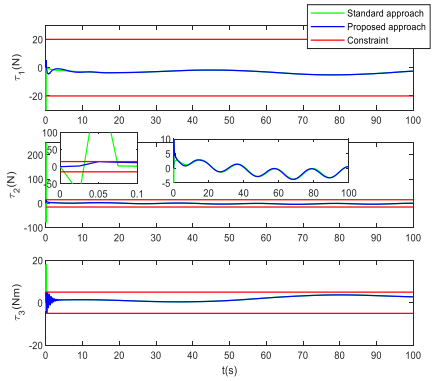

Fig. 20. Surge control force τ_1, sway control force τ_2, and yaw control moment τ_3.

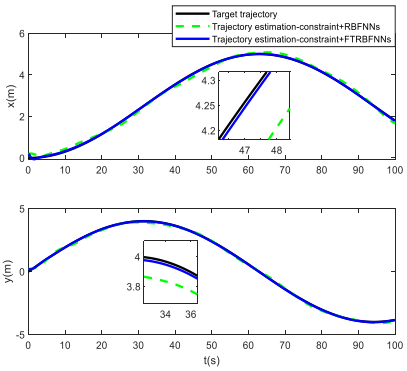

Fig. 21. Desired trajectory and desired trajectory estimation.

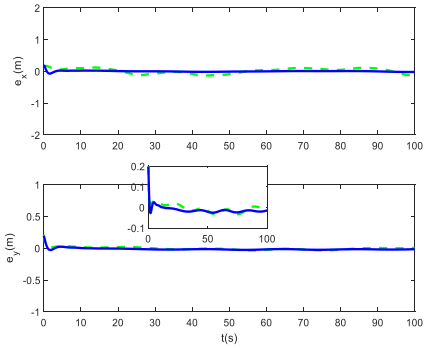

Fig. 22. Desired trajectory estimation and desired trajectory error e_x, e_y.

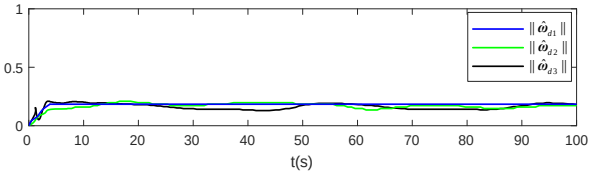

Fig. 23. The 2-norm curves of estimate trajectory parameters $\|\hat{\omega}_{d1}\|$, $\|\hat{\omega}_{d2}\|$, $\|\hat{\omega}_{d3}\|$.

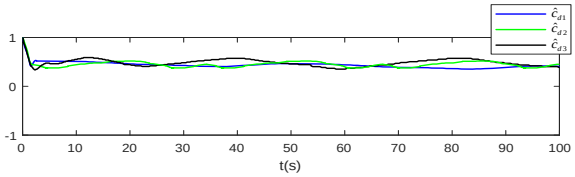

Fig. 24. The response curves of estimate trajectory parameters $\hat{c}_1$, $\hat{c}_2$, $\hat{c}_3$.

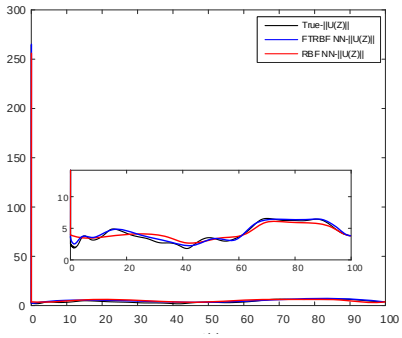

Fig. 25. System uncertainties approximation comparison.

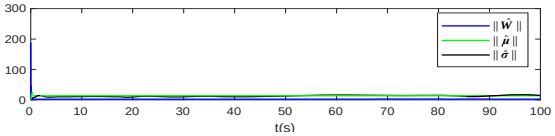

Fig. 26. The 2-norm curves of neural network estimation weight $\|\hat{\boldsymbol{W}}\|$, Gaussian function center estimation value $\|\hat{\boldsymbol{\mu}}\|$ and width estimation value $\|\hat{\boldsymbol{\sigma}}\|$.

Fig. 15 shows that both approaches can track the trajectory in the xy plane, further from Fig. 16 and Fig. 18 shows both approaches can make the system actual position and speed safely operate within the constraints. Fig. 17 and Fig. 19 shows that the error z_{11}, z_{12}, z_{21} and z_{22} transient and steady-state changes are slightly better than the proposed approach under the standard approach, and under the proposed approach error z_{13} transient state and steady state are better than standard approach, and z_{23} steady state is better than standard approach, and transient state is worse than the standard approach. This is due to the fact that a satisfactory tracking effect is obtained under various constraints. The standard approach can take a large control parameters to achieve a satisfactory tracking effect, but the control approach cannot satisfy the constraint requirements. This corresponding to Fig. 5 and Fig. 6. Furthermore, the control force will increase sharply under very large control parameters, which cannot satisfy the actual situation. This corresponds to Fig. 20.

Fig. 21 shows the desired trajectory and the estimation curve of the desired trajectory. It can be seen that the proposed approach can better estimate the desired trajectory under the action of the control parameters in Part 2. Fig. 22 corresponds to the error between estimation and desired in Fig. 21. Fig. 23 and Fig. 24 show the adaptive estimation parameters, and the estimation parameters are still bounded.

Fig. 25 also shows the FTRBFNNs proposed can better approximate system uncertainties. Fig. 26 shows the two norm variation curves of the FTRBFNNs. In summary of the simulation verification and the above, it can be seen that the proposed approach is effective and satisfies the control objective.

5. Conclusions

The backstepping combined with iBLF was constructed to directly handle the full-state constraints of the MSV system. The trajectory reconstruction approach was used to estimate the desired trajectory. Dynamic surface was applied to simplify derivation of virtual control law. Mean-value theorem combine with

hyperbolic tangent function were applied to approximate the saturation function. FTRBFNNs is more effective than RBFNNs in approximating the total uncertainties of the system.

With the proposed approach, we proved that all signals of the MSV closed-loop system are ultimately bounded. Simulations verified the effectiveness of the proposed approach. In the future work, the finite time/fixed time algorithm will be integrated into the unknown trajectory tracking control of dynamic positioning ship (DPS).

REFERENCES

[1]. *S. Yuan, Z. Liu, L. Zheng, et al.* "Event-based adaptive horizon nonlinear model predictive control for trajectory tracking of marine surface vessel", Ocean engineering, 2022.

[2]. *S. Yu, J. Lu, G. Zhu, et al.* "Event-triggered finite-time tracking control of underactuated MSVs based on neural network disturbance observer", Ocean engineering, no. 1, 2022, pp. 253.

[3]. *H. Xue, Wang. Yabin.* "A novel asymmetric barrier Lyapunov function-based fixed-time ship berthing control under multiple state constraints", Ocean Engineering , 2023, pp. 87-91.

[4]. *G. Deyang.* "Research on Trajectory Tracking and Obstacle Avoidance Planning Control of Driverless Vehicle Based on MPC", Automotive Test Reports, no. 15, 2023, pp. 55-57.

[5]. *F. Yang.* "Target Tracking Algorithm Based on Extended Kalman Filtering", Computer Knowledge and Technology, no. 24, 2022, pp. 18.

[6]. *W. Yanjie.* "Deep learning-based pedestrian tracking and trajectory prediction in extraordinary conditions", IEEE Trans. Neural. Netw., 2024, pp. 32-36.

[7]. *T. Kengpeng, et al.* "Control of nonlinear systems with time-varying output constrains", Automatica., **vol. 47**, no. 11, 2011, pp. 2511-2516.

[8]. *R. Beibei, et al.* "Adaptive neural control for output feedback nonlinear systems using a barrier Lyapunov function", IEEE Trans. Neural. Netw., **vol. 21**, no. 8, 2010, pp. 1339-1345.

[9]. *Z. Yin, H. Wei and Y. Chengguang*, "Tracking control of a surface vessel with full-state constraints", Int. J. Syst. Sci., **vol. 48**, no. 3, 2017, pp. 535-546.

[10]. *W. Libing, et al.* "Neural Network Adaptive Tracking Control of Uncertain MIMO Nonlinear Systems With Output Constraints and Event-Triggered Inputs", IEEE Trans. Neural. Netw., 2020, pp. 1-13.

[11]. *T. Zhongliang, et al.* "Robust Adaptive Neural Tracking Control for a Class of Perturbed Uncertain Nonlinear Systems with State Constraints", IEEE Trans. Syst. Man. Cybern., **vol. 46**, no. 12, 2016, pp. 1618-1629.

[12]. *D. Jialu, et al.* "Robust dynamic positioning of ships with disturbances under input saturation", Automatica., no. 73, 2016, pp 207-214.

[13]. *T. Zhongliang, et al.* "Adaptive neural control for an uncertain robotic manipulator with joint space constraints", Int. J. Control., **vol. 89**, no. 7, 2016, pp. 1428-1446.

[14]. *T. I. Fossen*, Handbook of Marine Craft Hydrodynamics and Motion Control, John Wiley & Sons, Chichester, UK, 2011.

[15]. *Z. Zewei, et al.* "Adaptive Trajectory Tracking Control of a Fully Actuated Surface Vessel With Asymmetrically Constrained Input and Output", IEEE Trans. Control. Syst. Technol., **vol. 26**, no. 5, 2018, pp. 1851-1859.

[16]. *W. Yijian, et al.* "Research on BP Neural Network PID Control Algorithm for Magnetic Bearing", Machine Build. Auto., **vol. 52**, no. 4, 2023, pp. 177-180.

[17]. *W. Huanqing, et al.* "Robust adaptive fuzzy tracking control for pure-feedback stochastic nonlinear systems with input constraints", IEEE Trans. Cybern., **vol. 43**, no. 6, 2013, pp. 2093-2104.
[18]. *R. Skjetne, T. I. Fossen and P. V. Kokotovic*, "Adaptive maneuvering with experiments for a model ship in a marine control laboratory", Automatica., **vol. 41**, no. 2, 2005, pp. 289-298.
[19]. *Y.Yang, et al.* "A trajectory tracking robust controller of surface vessels with disturbances uncertainties", IEEE Trans. Control. Syst. Technol., **vol. 22**, no. 4, 2014, pp. 1511-1518.
[20]. *T. Kengpeng, et al.* "Barrier Lyapunov functions for the control of output-constrained nonlinear systems", Automatica., **vol. 45**, no. 4, 2009, pp. 918-927.
[21]. *W. Changfeng, et al.* "Robust adaptive control of uncertain nonlinear systems in the presence of input saturation and external disturbance", IEEE Trans. Auto. Control., **vol. 56**, no. 7, 2011, pp. 1672-1678.
[22]. *H. Sunan, et al.* "Further results on adaptive control for a class of nonlinear systems using neural networks", IEEE Trans. Neural Networks., **vol. 14**, no. 3, 2003, pp.719-722.
[23]. *L. Yongchao, Z. Qidan and W. Lipeng*, "Practical finite time control for surface ships with output constraints", CTA., **vol. 40**, no. 2, 2023, pp. 7.

APPENDIX A

A.1: Preliminary

Definition 1: The BLF $V(x)$ defined in [20].

Definition 2: For any $x \in \mathbb{R}$, $tanh(x): \mathbb{R} \to \mathbb{R}$ is defined as $\tanh(x) = e^{x} - e^{-x} / e^{x} + e^{-x}$

Definition 3 : The Nussbaum-type function $N(s)$ define in [21].

Lemma 1 : The properties of function $N(s)$ can be found in reference [21].

Lemma 2 [13]: The functional $V_{x_{1,j}}\ (i = 1, \cdots, n)$, described as $V_{x_{1,i}}(z_i(t), q_{d_i}(t)) = \int_0^{z_i} \frac{\sigma k_{c_i}^2 d\sigma}{(k_{c_i}^2 - (\sigma + q_{d_i})^2)}$, satisfies $V_{x_{1,i}} \le \frac{k_{c_i}^2 z_i^2}{k_{c_i}^2 - x_{1,i}^2}$, where $k_{c_i} > 0$ is constant; $z_i = x_{1,i} - q_{d_i}$; variable $\sigma = \theta z_i(t)$; $x_{1,i}$ satisfies $| x_{1,i} | < k_{c_i}$.

Lemma 3 [22]: For adaptive law of form $\dot{\hat{\boldsymbol{W}}}_i = \boldsymbol{\Gamma}_i [\boldsymbol{S}_i \boldsymbol{z}_2(i) - \nu_i | \boldsymbol{z}_2(i) | \hat{\boldsymbol{W}}_i]$, there exists a compact set $\Omega_0 := \{\hat{\boldsymbol{W}}_i \mid \left\| \hat{\boldsymbol{W}}_i \right\| \le s_i / \nu_i\}$, where $\| \boldsymbol{S}_i \| \le s_i$, $\hat{\boldsymbol{W}}_i(0) \in \Omega_0$, $\forall t \ge 0$.

NN Approximation: The FTRBFNNs are define in [23]. 原价注册